Supplementary Information

Magnesium-iron modified sludge biochar for methyl orange removal via adsorption and periodate-based advanced oxidation

Hongyun Sun, Duo Meng*, Hehe Yang , Ziming Liu

School of Civil and Architectural Engineering, Liaoning University of Technology, Jinzhou 121000, China

Total 15 pages including 3 Texts, 2 Figures, and 2 Tables.

* Corresponding author. Email address: mengduo39@163.com

List of Supplementary Information:

1 Texts

2 Figures

3 Tables

Text S1. Chemicals and reagents.

The dewatered sludge used in this study was taken from the Daughter River Wastewater Treatment Plant in Jinzhou, Liaoning. MO ($C_{14}H_{14}N_3SO_3Na$, 98%), sodium periodate (SP), methanol (MeOH), sodium hydroxide (NaOH), hydrochloric acid (HCl), tert-butanol (TBA), furfuryl alcohol (FFA), phenol (PhOH), dimethyl sulfoxide (DMSO) and para-benzoquinone (PBQ) were purchased from Shanghai McLean Biochemical Co. Ferric chloride hexahydrate ($FeCl_3 \cdot 6H_2O \geq 99\%$) was purchased from Tianjin Damao Chemical Reagent Factory, sodium chloride (NaCl), sodium sulfate (Na_2SO_4) was purchased from Xilong Science Co., Ltd, sodium nitrate ($NaNO_3$) was purchased from Tianjin Golden Glass Chemical Experimental Equipment Sales Co. $MgCl_2 \cdot 6H_2O > 98\%$), Sodium dihydrogen phosphate (NaH_2PO_4) and Sodium bicarbonate ($NaHCO_3$) were purchased from Shanghai Sinopharm Chemical Reagent Co.

Text S2. Adsorption and catalysis experiments

Adsorption kinetic studies were conducted by dispersing 30 mg of biochar into 100 mL of a 30 mg/L MO solution. Aliquots were collected at predetermined time intervals (1, 3, 5, 10, 20, 40, 60, 80, 100, 120, 180, and 240 min), filtered through 0.45 μm membrane filters, and analyzed for residual MO concentration using UV-vis spectrophotometry. Adsorption isothermal and thermodynamic experiments were performed at 25 °C, 35 °C, and 45 °C, respectively. In these experiments, 30 mg of biochar was added to 100 mL of MO solutions with varying initial concentrations (20-100 mg/L). After 240 min of reaction time, samples were collected, filtered through 0.45 μm membranes, and analyzed for MO concentration.

Performance optimization experiments were carried out by adding 15 mg of SBC-a to 100 mL of a 30 mg/L MO solution. Beakers were wrapped with aluminum foil to prevent light exposure during the experiments. The pH of the MO solution was adjusted using 0.1 M NaOH or 0.1 M HCl. Unless specified for pH-effect studies, the initial pH was maintained at 3.0 in all experiments. Adsorptive removal was conducted under magnetic stirring for 30 min, with samples collected at 15-min intervals, filtered through 0.45 μm membranes, and analyzed for MO concentration. The oxidative reaction was initiated by the addition of 2 mL of 40 mM SP solution. Subsequently, 2 mL aliquots were withdrawn at specified time points (15, 30, 45, 60, 75, 90, 105, and 120 min), immediately filtered through 0.45 μm membrane filters, and analyzed to determine the remaining MO concentration. Unless otherwise stated, all batch experiments were conducted at 20 ± 2 °C, with a target initial MO concentration of 30 mg/L, a biochar dosage of 0.15 g/L (i.e., 15 mg in 100 mL), an SP concentration of 0.8 mM, and a total solution volume of 100 mL. At equilibrium, the maximum adsorption of MO q_e (mg/g) is consistent with Eq. (1).

$$q_e = \frac{c_0 - c_e}{m} v \tag{1}$$

where q_e (mg/g) denotes the equilibrium adsorption amount; C_0 (mg/L) and C_e (mg/L) denote the initial and equilibrium concentrations of MO, respectively. V (L) is the volume of the adsorbed solution, and m (g) represents the amount of adsorbent.

The adsorption kinetics were described using the pseudo-first-order model Eq. (2) and pseudo-second-order model Eq. (3). The adsorption process was described by the intraparticle diffusion model Eq. (4).

$$\ln(q_e - q_t) = \ln q_e - k_1 t \tag{2}$$

$$\frac{\mathrm{t}}{q_\mathrm{t}} = \frac{1}{k_2 q_\mathrm{e}^2} + \frac{\mathrm{t}}{q_\mathrm{e}} \tag{3}$$

$$q_\mathrm{t} = k_\mathrm{p} t^{1/2} + c \tag{4}$$

where q_e (mg/g) denotes the amount of MO adsorbed at equilibrium, and q_t (mg/g) denotes the amount of MO adsorbed at time t. k_1 (min^{-1}), k_2 g/mg·min), and k_p mg/(g·$\mathrm{min}^{1/2}$) denote the pseudo-first-order model, pseudo-second-order model, and the intra-particle diffusion rate constants, respectively. c stands for the boundary layer thickness constant.

The isotherm experimental data were fitted using the Langmuir model Eq. (5) and the Freundlich model Eq. (6).

$$q_\mathrm{e} = \frac{q_\mathrm{max} K_\mathrm{L} c_\mathrm{e}}{1 + K_\mathrm{L} c_\mathrm{e}} \tag{5}$$

$$q_\mathrm{e} = K_\mathrm{F} c_\mathrm{e}^{1/\mathrm{n}} \tag{6}$$

Where K_L (L/mg) and q_max (mg/g) represent the Langmuir adsorption energy and the maximum adsorption capacity, respectively; K_F (mg/g)(L/mg) 1/n and n represent the intensity indexes related to the Freundlich model constants and the strength of the adsorption, respectively. c_e (mg/L) and $\mathrm{q_e}$ (mg/g) represent the liquid-phase concentration and the equilibrium adsorption capacity after adsorption, respectively.

The thermodynamic equations were used to determine whether the adsorption was a spontaneous or non-spontaneous, absorptive or exothermic, stochastic increasing or decreasing process as shown in Eq. (7) ~ Eq. (9).

$$\Delta G = -RT\ln K_{\mathrm{L}} \tag{7}$$

$$\ln K_{\mathrm{L}} = \frac{\Delta S}{R} - \frac{\Delta H}{RT} \tag{8}$$

$$K_{\mathrm{L}} = \frac{q_{\mathrm{e}}}{c_{\mathrm{e}}} \tag{9}$$

where ΔG is the Gibbs free energy change, kJ/mol, ΔH is the enthalpy change, kJ/mol, ΔS is the entropy change, kJ/(mol·K), K is the thermodynamic equilibrium constant (L/g), and qe and ce denote the equilibrium adsorption amount and concentration at equilibrium, respectively.

Text S3. Characterization methods

The morphological characteristics of the biochar were analyzed using scanning electron microscopy (SEM, Zeiss Sigma 500, Germany). Elemental composition and content analysis of biochar were performed using Energy Dispersive Spectrometer (EDS, German Zeiss Supra 55). Surface functional groups were identified by Fourier transform infrared spectroscopy (FTIR, Thermo Fisher Nicolet 6700, USA). The specific surface area, total pore volume, and average pore size of the biochar samples were determined via nitrogen adsorption-desorption measurements using a BET surface area analyzer (Kantar Autosorb-iQ2, USA). Crystalline phases were characterized by X-ray diffraction (XRD, D/max-2550VB+/PC, Rigaku, Japan), and elemental composition was assessed using X-ray photoelectron spectroscopy (XPS, PHI-5300 ESCA, PerkinElmer, USA). Reaction intermediates were identified through liquid chromatography-mass spectrometry (LC/MS, 6530 Q-TOF, Agilent, USA). Chromatographic separation was performed on a Hypersil GOLD column (150 mm×4.6 mm, 3.5 μm) with binary gradient elution, employing mobile phases A (0.01 mol/L ammonium acetate) and B (acetonitrile). Full-scan mass spectra were acquired over a range of 50-1200 m/z.

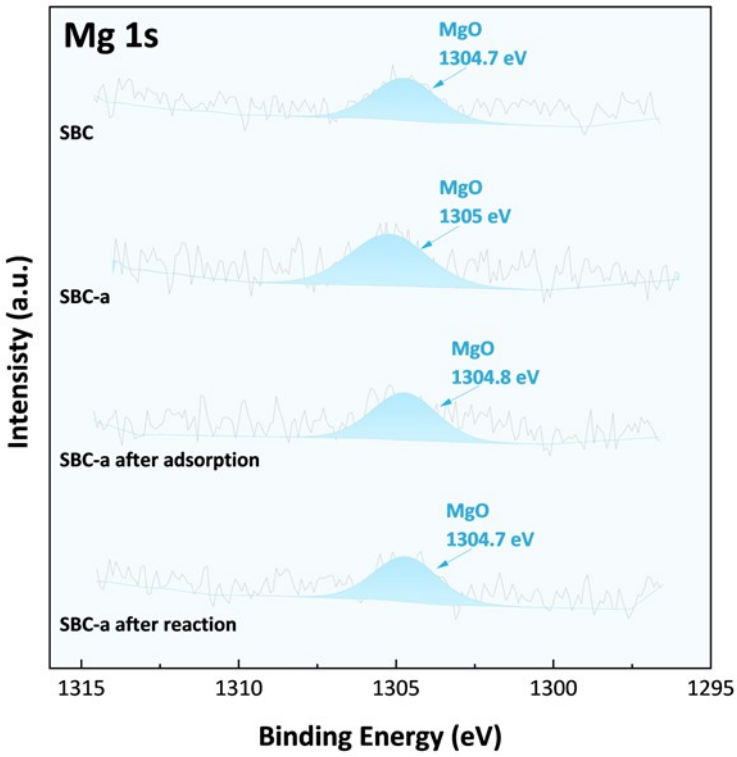

Fig. S1. XPS spectra of Mg1s.

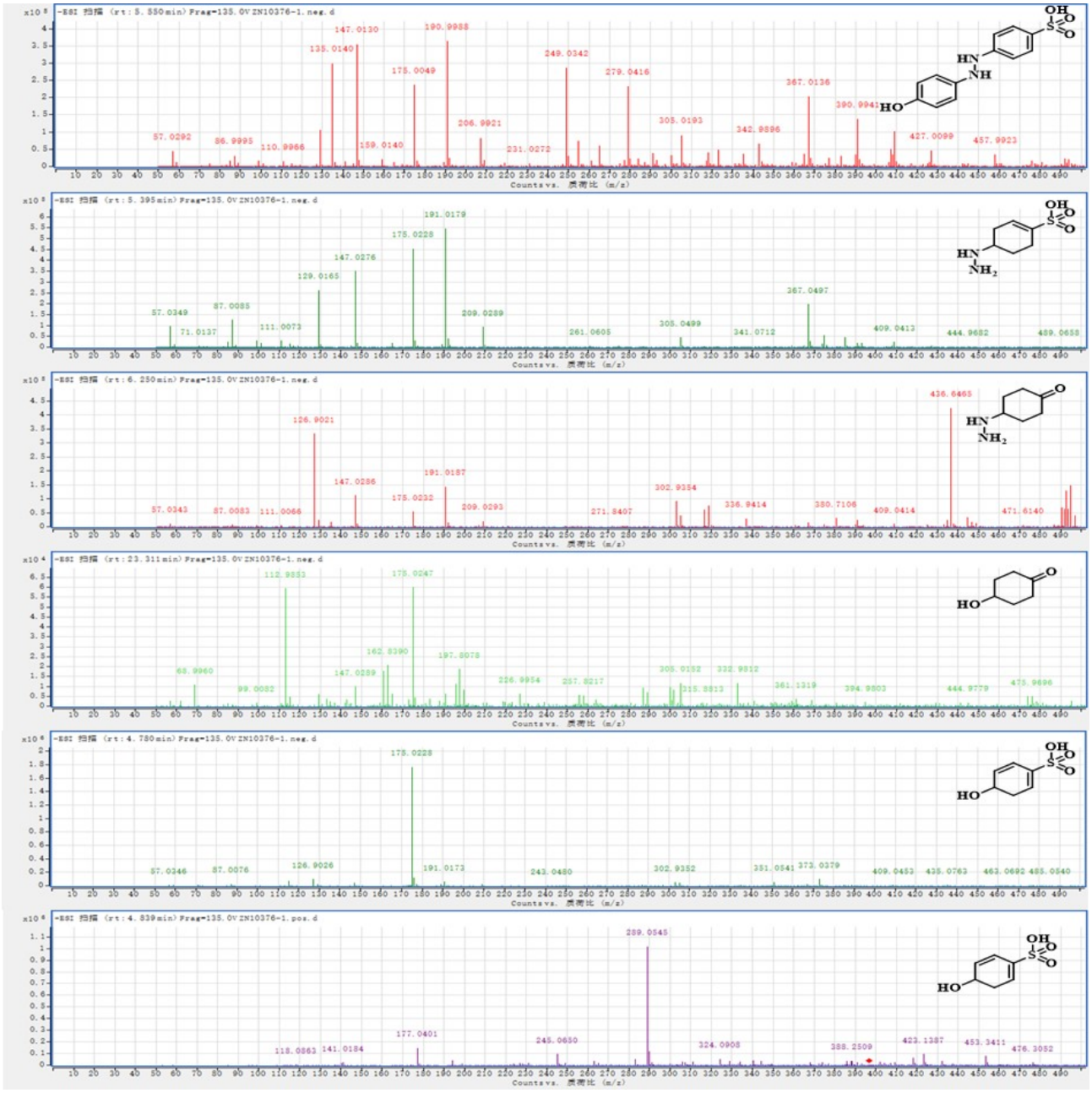

Fig.S2. The mass spectra of MO and its intermediates.

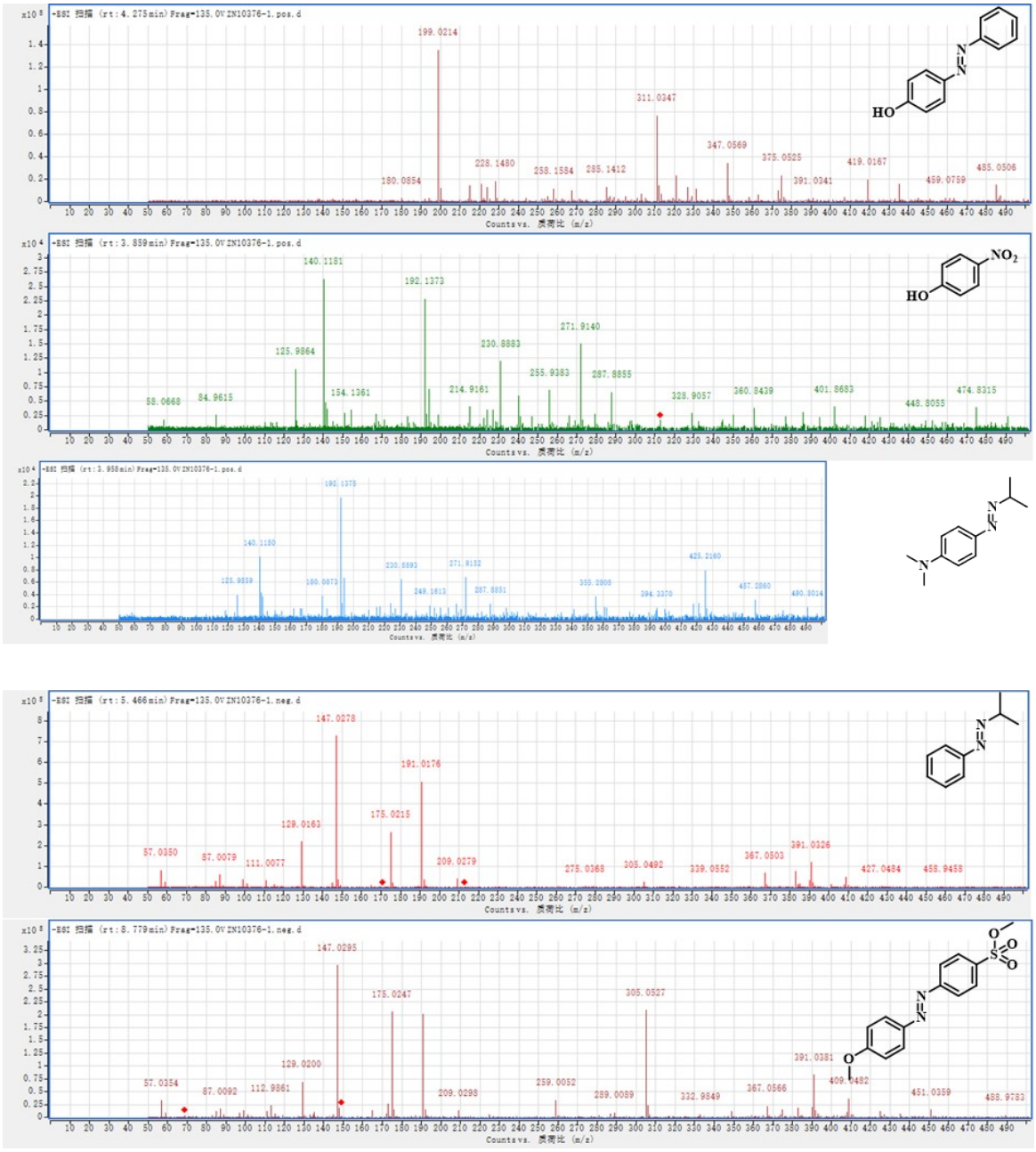

Fig.S3. The mass spectra of MO and its intermediates.

Table S1. MO rate constants and R^2 values under different reaction conditions

Parameters		$k_{obs}(min^{-1})$	R^2
Biochar samples	SBC	0.0048	0.999
	MgSBC	0.006	0.996
	FeSBC	0.0102	0.999
	SBC-a	0.0179	0.998
PH	3	0.0185	0.997
	5	0.047	0.983
	7	0.0032	0.962
	9	0.0019	0.968
SBC-a dosage (g/L)	0.1	0.006	0.938
	0.15	0.0189	0.992
	0.2	0.0303	0.982
	0.25	0.0365	0.946
SP dosage (mM)	0.4	0.0069	0.989
	0.8	0.167	0.998
	1.2	0.232	0.999
Anion	cl^-	0.0253	0.998
	NO_3^-	0.0267	0.999
	SO_4^{2-}	0.02	0.992
	HCO_3^-	0.0023	0.947
	$H_2PO_4^-$	0.0178	0.996
Quencher	TBA 50mM	0.0121	0.997
	FFA 50mM	0.00298	0.941

PBQ 5mM	0.0046	0.992
PhoH 5mM	0.0046	0.982
MeoH 50mM	0.0057	0.993
DMSO 50mM	0.0065	0.993
control	0.0186	0.997

Table S2. MO Degradation Product Data

产物	保留时间（min）	分子式	m/z	结构式
P1	5.550	$C_{12}H_{12}N_2O_4S$	279 $[M-H]^-$	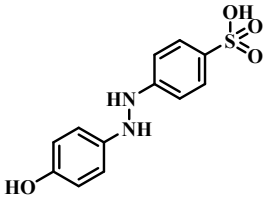
P2	5.395	$C_6H_{12}N_2O_3S$	191 $[M-H]^-$	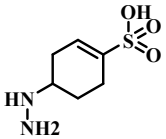
P3	6.250	$C_6H_{12}N_2O$	127 $[M-H]^-$	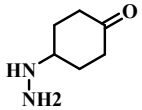
P4	23.311	$C_6H_{10}O_2$	113 $[M-H]^-$	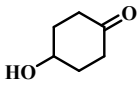
P5	4.780	$C_6H_8O_4S$	177 $[M+H]^+$ 175 $[M-H]^-$	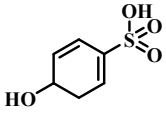
P6	4.275	$C_{12}H_{10}N_2O$	199 $[M+H]^+$	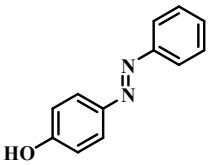
P7	3.859	$C_6H_5NO_3$	140 $[M+H]^+$	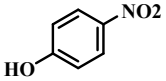
P8	3.958	$C_{11}H_{17}N_3$	192 $[M+H]^+$	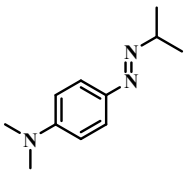

P9	5.466	$C_9H_{12}N_2$	147 $[M-H]^-$	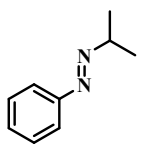
P10	8.779	$C_{14}H_{14}N_2O_4S$	305 $[M-H]^-$	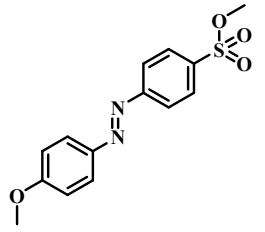

References:

[1] Xiao H, Shahab A, Li J, et al. Distribution, ecological risk assessment and source identification of heavy metals in surface sediments of Huixian karst wetland, China[J]. Ecotoxicology and Environmental Safety, 2019, 185: 109700.

[2] Du L, Ahmad S, Liu L, et al. A review of antibiotics and antibiotic resistance genes (ARGs) adsorption by biochar and modified biochar in water[J]. Science of the total environment, 2023, 858: 159815

[3] Jung K W, Lee S, Lee Y J. Synthesis of novel magnesium ferrite ($MgFe_2O_4$)/biochar magnetic composites and its adsorption behavior for phosphate in aqueous solutions[J]. Bioresource technology, 2017, 245: 751-759.

[4] Jiang W, Cai Y, Liu D, et al. Enhanced adsorption performance of oxytetracycline in aqueous solutions by Mg-Fe modified suaeda-based magnetic biochar[J]. Environmental Research, 2024, 241: 117662.

[5] Peng, Hongbo, et al. "Enhanced adsorption of Cu (II) and Cd (II) by phosphoric acid-modified biochars." Environmental Pollution 229 (2017):

[6] Li, Hanbing, et al. "Efficient simultaneous phosphate and ammonia adsorption using magnesium-modified biochar beads and their recovery performance." Journal of Environmental Chemical Engineering 11.5 (2023): 110875.

[7] Yamashita, Toru, and Peter Hayes. "Analysis of XPS spectra of Fe^{2+} and Fe^{3+} ions in oxide materials." Applied surface science 254.8 (2008): 2441-2449.

[8] Li, Xiaowan, et al. "Activation of periodate by granular activated carbon for acid orange 7 decolorization." Journal of the Taiwan Institute of Chemical Engineers 68 (2016): 211-217.

[9] Lee, Changha, and Jeyong Yoon. "Application of photoactivated periodate to the decolorization of reactive dye: reaction parameters and mechanism." Journal of Photochemistry and Photobiology A: Chemistry 165.1-3 (2004): 35-41.

[10] He L, Lv L, Pillai S C, et al. Efficient degradation of diclofenac sodium by periodate activation using Fe/Cu bimetallic modified sewage sludge biochar/UV system[J]. Science of the Total Environment, 2021, 783: 146974.

[11] Chadi, Nor Elhouda, et al. "Influence of mineral water constituents, organic matter and water matrices on the performance of the H_2O_2/IO^{4-}-advanced oxidation process." Environmental Science: Water Research & Technology 5.11 (2019): 1985-1992.